Polymer 51 (2010) 1599–1607

Contents lists available at ScienceDirect

Polymer

journal homepage: www.elsevier.com/locate/polymer

Polystyrene as a versatile nucleating agent for polypropylene

Andrew Phillips*, Peng-Wei Zhu, Graham Edward

Cooperative Research Centre (CRC) for Polymers, Department of Materials Engineering, Monash University, Vic 3800, Australia

ARTICLE INFO

Article history:
Received 14 October 2009
Received in revised form
15 January 2010
Accepted 3 February 2010
Available online 10 February 2010

Keywords:
Simultaneous wide and small angle X-ray scattering
Time resolved
Crystallisation

ABSTRACT

The morphology of isotactic polystyrene (iPS) particles which had been compounded into an isotactic polypropylene (iPP) matrix was varied in-situ by selective heat treatment to be either amorphous ($iPS_{amorphous}$) or semicrystalline ($iPS_{crystalline}$). The influence of iPS morphology on the quiescent and shear-induced isothermal crystallisation of iPP was then studied using differential scanning calorimetry (DSC), in-situ simultaneous small and wide angle X-ray scattering (SAXS/WAXS) and polarised optical microscopy (POM). In the quiescent condition $iPS_{crystalline}$ was found to selectively nucleate the β phase while $iPS_{amorphous}$ nucleated the α phase of iPP. Compared to the control sample ($iPP_{control}$), the presence of both morphologies of iPS increased the number of shear-induced oriented crystal precursors that form as a result of the step shear. During isothermal crystallisation the shear-induced nuclei promote oriented α form crystal growth, accelerate the crystallisation kinetics and ultimately swamp the effect of the nucleating particles present.

1. Introduction

Natta and Corfidini showed that the usual crystal form of isotactic polypropylene (iPP) has each polymer molecule arranged as a 3_1 helix [1]. The helix is chiral and can exist in either the right or left hand configuration. This chirality allows for four different crystalline phases: α (monoclinic) [1], β (trigonal) [2–4], γ (orthorhombic) [5] and the smectic phase [1]. α-iPP is by far the most common and occurs under a wide variety of crystallisation conditions. β-iPP has received considerable attention due to its promising mechanical properties, such as improved toughness and elongation at break [6–8]. β-iPP is thermodynamically less stable and is therefore more difficult to obtain under conditions typically found in industrial processes.

Numerous methods have been developed to produce significant quantities of β phase such as: crystallisation in a temperature gradient [9]; shear-induced crystallisation [10–14], particularly in oscillation mode [15–17]; and by the addition of specific β nucleating agents [16,18–23]. Of these methods, large fractions of β-iPP are most easily attained by the addition of specific β nucleating agents. Historically these agents have been derived from low molecular weight crystallisable compounds, which can broadly be divided into two categories. The first category includes aromatic compounds such as γ-quinacridone [20] (Red Pigment E3B), while the second category includes compounds derived from group IIA metal salts such as LaC and $CaCO_3$ [18] and Ca salts of pimelic and suberic acid [18,19]. The selectivity of these agents can be described by a two dimensional lattice matching theory [24–27]. Central to this theory is that a reasonable epitaxial match, at least within 10%, occurs between the repeat distance in the iPP unit cell and the corresponding nucleating surface. Recently, an amorphous polymeric nucleating agents, styrene acrylonitrile (SAN) and polystyrene (PS) were shown to also selectively nucleate β-iPP [22,23]. However, it is unclear how an epitaxial theory could explain the nucleation mechanism of these amorphous polymers. These polymers have the advantage of being relatively cheap and easy to process and therefore show good commercial potential. However, any explanation for the nucleation mechanism of these amorphous polymers is at best tentative.

The methyl groups of the iPP would most likely interact with the phenyl groups of PS [26] and therefore the arrangement of the phenyl groups would be important to understanding any epitaxial relationship between the two. The structure of amorphous polystyrene has been extensively studied [28–34]. The most comprehensive model proposed to date shows the phenyl groups micro-segregate into stacks [34]. Although the stacks are disordered, the phenyls within the stacks not only show significant positional registration with neighbouring phenyls within the same stack but neighbouring stacks show also significant positional registration with each other. The repeat distance between adjacent phenyl groups in the same stack is ~5 Å. Isotactic polystyrene (iPS), being a stereoregular polymer, allows the iPS molecules to

* Corresponding author. Tel.: +61 421 607 983; fax: +61 3 9905 4940.
E-mail address: andyphil21@gmail.com (A. Phillips).

0032-3861/$ – see front matter © 2010 Elsevier Ltd. All rights reserved.
doi:10.1016/j.polymer.2010.02.005

crystallise in the form of a 3_1 helix [35]. Micro-segregation of the phenyls into regular stacks is also a feature of crystalline iPS, with the repeat distance between adjacent phenyl groups within each stack being 6.65 Å. If epitaxy is significant, the change in the arrangement of phenyls between the amorphous and crystalline states of iPS should lead to a change in iPP crystallisation behaviour. Accordingly, in this study the morphology of iPS particles embedded in an iPP matrix were varied to be either semicrystalline ($iPS_{crystalline}$) or amorphous ($iPS_{amorphous}$) and their influence on the isothermal quiescent crystallisation of iPP was then studied.

Shearing the melt prior to the onset of crystallisation further complicates the crystallisation of iPP in the presence of nucleating agents. Most importantly shear increases the number of shear-induced oriented crystal precursors [36–40] which can then template the formation of oriented crystalline and lamellar structures [39,40]. The addition of common nucleating agents has been found to increase the density of the oriented crystal precursors for a given set of crystallisation conditions [41] and it is suspected that their presence can significantly reduce the activity of any nucleating agents present [16,18]. For these reasons, crystallisation after a moderate step shear was also studied.

2. Experimental

2.1. Sample preparation

The matrix polymer used in this study was an iPP homopolymer manufactured by the Borealis group with $M_w = 367{,}000$ g/mol and $M_n = 74{,}000$ g/mol. The polymeric nucleating agent used was a fine powder of iPS (>90% isotactic) manufactured by Scientific Polymer Products Inc. with $M_w = 400{,}000$ g/mol. The iPS was heated in a vacuum oven at 180 °C for 5 h to induce a high degree of crystallinity then sieved through a 100 μm mesh to further reduce the average grain size of the particles. 2 wt% of the refined iPS powder was compounded into molten iPP at 190 °C for 10 min at 60 RPM in a Haake Rheocord 90 batch mixer. This master batch was then compression moulded into sheets 1.5 mm thick at 190 °C for 5 min.

2.2. Thermal–shear profile

A Linkam CSS450 shear cell was used to control the thermal–shear profile. To ensure consistent temperature between the X-ray and optical set ups, external temperature calibrations were used. Two thermal pre-treatments were applied above and below the crystalline melting point of iPS ($T^0_{m(iPS)} = 242$ °C) [42] to yield samples where the morphology of the iPS was predominantly amorphous or semicrystalline. Amorphous iPS in a matrix of iPP ($iPP(iPS_{amorphous})$) was produced by heating the master batch to 280 °C for 3 min then quickly cooling it to room temperature at 30 °C/min, while crystalline iPS in a matrix of iPP ($iPP(iPS_{crystalline})$) was produced by heating the material to 200 °C for 3 min before cooling too room temperature. Control material ($iPP_{control}$) containing no nucleating agent was prepared under the same conditions as $iPP(iPS_{crystalline})$ and $iPP(iPS_{amorphous})$. The crystallisation kinetics of the $iPP_{control}$ material prepared by both routes was found to be similar showing degradation of the iPP matrix was not significant under the experimental conditions. All samples were then reheated to 200 °C, compressed to the required gap thickness and held there for at least 3 min to eliminate the previous thermal history of the iPP matrix. Samples were cooled to the isothermal crystallisation temperature of 135 °C at 30 °C/min. Crystallisation from the quiescent melt and after a moderate step shear with a shear rate of 80 s^{-1} and duration of 1 s were studied. In all cases the samples were held at the crystallisation temperature for long enough for the crystallisation rate to be effectively negligible. Samples were then cooled at 30 °C/min to room temperature.

Additional heat treatments, identical to those experienced by $iPP(iPS_{crystalline})$ and $iPP(iPS_{amorphous})$ were performed to prepare iPS samples of sufficient size for ex-situ X-ray analysis. The crystalline iPS material was designated ($iPS_{crystalline}$), while the amorphous iPS material was designated ($iPS_{amorphous}$).

2.3. Optical microscopy

Polarised optical micrographs (POMs) were taken on a Nikon 80i microscope using a Nikon DS-Fi1 CCD camera at a shear cell gap thickness of 50 μm.

2.4. Differential scanning calorimetry

Differential scanning calorimetry (DSC) experiments were performed on the fully crystallised iPP samples using a Perkin–Elmer DSC-7 at heating rates of 10 °C/s and under a nitrogen atmosphere. Sample size was ~5 mg. Pure indium and zinc references were used for calibration. Heating scans were also performed on the ex-situ iPS material which had experienced similar conditions to that which the compounded material experienced in the shear cell. Enthalpy of fusion, ΔH, was determined by integrating the area under the baseline corrected thermogram. Percentage crystallinity of iPS was calculated from the ratio of $\Delta H/\Delta H_0^{iPS}$ where ΔH for iPS was taken as 86.59 j/g [43]. The density of the crystalline and amorphous phases were taken as 1.08 g/cm^3 [35] and 1.056 g/cm^3 [30] respectively.

2.5. X-ray scattering

Simultaneous two dimensional wide and small angle X-ray scattering experiments (SAXS & WAXS) were performed on the SAXS/WAXS beamline at the Australian Synchrotron, Fig. 1. The setup allowed for in-situ investigations with a considerable amount of the scattering intensity around the azimuth ($\phi \sim 80°$) in the WAXS region (Polaris CCD 2D detector) to be captured whilst simultaneously capturing complete SAXS patterns (MAR CCD 2D detector). The shear cell was adapted for use with X-ray radiation. The bottom plate had three slots allowing X-rays to be introduced to the sample. The top plate had a narrow 3 mm diameter aperture allowing scattered X-rays to pass. Thin films of Kapton™ ~50 μm were used to contain the sample between the top and bottom plates. A shear cell gap thickness of 500 μm was used. Beam dimensions of 250 × 150 μm, a wavelength of $\lambda = 1.48$ Å, and an exposure time of 1 s were employed throughout the experiment. Scattering without the specimen was also recorded to enable background correction. All images were normalised to the main

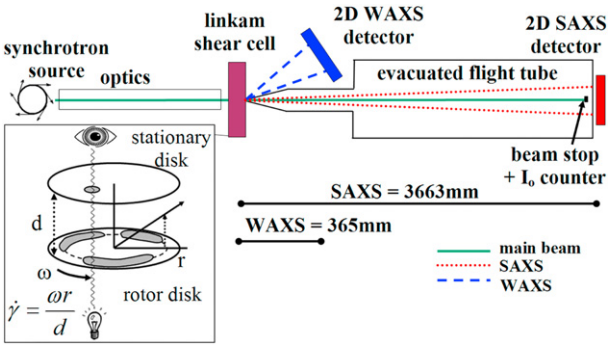

Fig. 1. Diagram of the simultaneous 2D WAXS/SAXS setup used at the Australian Synchrotron.

beam intensity which was measured by a scintillation counter mounted in the beam stop. The SAXS15id program was used to reduce the 2D data.

Additional WAXS experiments were performed on ex-situ iPS samples that had been subjected to similar thermal treatments to that experienced in the shear cell. The experiments were performed at the Australian National Beamline Facility (ANBF), a synchrotron beamline at the Photon Factory in Tsukuba, Japan. Details of the experimental setup have been reported in previous papers [40,41]. Beam dimensions were 200 × 200 μm, the exposure time was 300 s, and the wavelength was 2 Å. The camera length was 111 mm and image plates were used as the detection system. The Nika software program was used to reduce the 2D data.

Uncertainty in the parameters measured by X-ray and DSC methods was assessed by calculating the standard error in the measurement and the 95.4% confidence interval was reported.

3. Results

3.1. Morphology of iPS particles

A survey was conducted to establish the homogeneity and dispersion of iPS particles in the iPP matrix and to investigate the influence of the selective heat treatment on the morphology of the iPS particles. The distribution of equivalent spherical diameters (D) of the $iPS_{crystalline}$ and $iPS_{amorphous}$ particles in the iPP matrix was determined by taking 10 POMs of each sample and applying standard image analysis techniques to determine D for each particle. The results are presented in Fig. 2a. The analysis showed a very similar distribution of diameters for iPS particles in both iPP($iPS_{amorphous}$) and iPP($iPS_{crystalline}$) material with the average equivalent spherical diameter D_{ave} for both being ~16 μm. The influence of the selective thermal pre-treatments on the morphology of the iPS particles can be illustrated by following the changes that occurred to same iPS particle after heat treatment. Initially, the iPS particle embedded in the iPP matrix was heated to 200 °C for 3 min (iPP($iPS_{crystalline}$)), Fig. 2b. In this condition the particle showed high birefringence and was of irregular shape. The same particle was then heated to 280 °C for 3 min (iPP($iPS_{amorphous}$)), Fig. 2c. After this treatment the particle lost its birefringence and tended to became slightly more rounded in appearance.

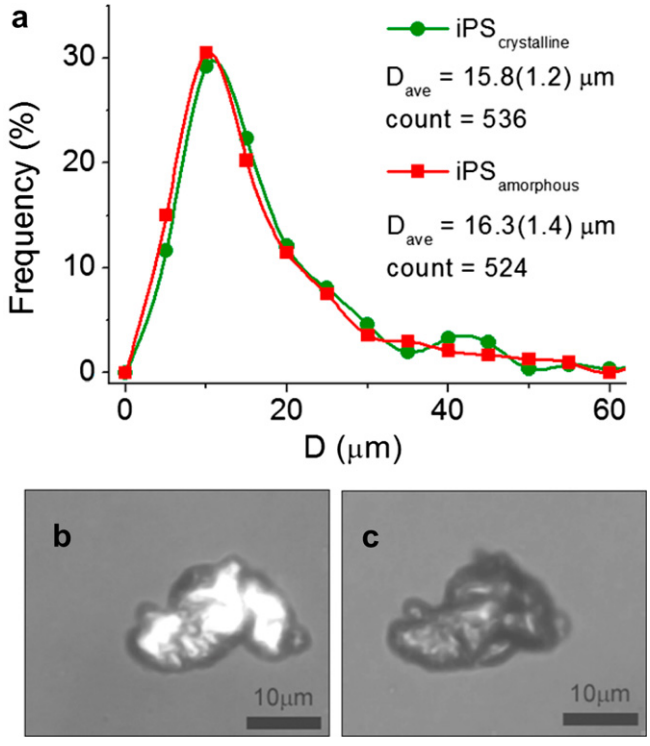

Fig. 2. (a) Distribution of the equivalent spherical diameter (D) for iPS particles in iPP(iPScrystalline) and iPP(iPSamorphous) material. POM image of a typical iPS particle in the iPP matrix held at (b) 200 °C for 3 min, and (c) the same particle held at 280 °C for 3 min.

Fig. 3 shows the scattered intensity versus 1D scattering vector ($q = 4\pi\sin\theta/\lambda$; where θ is the scattering angle and λ is the incident wavelength) of the two iPS samples given similar thermal profiles to that which the master batch of 2 wt% iPS in iPP was subjected in the shear cell. For clarity the $iPS_{crystalline}$ curve is offset from $iPS_{amorphous}$. The WAXS profile of $iPS_{amorphous}$ shows two broad amorphous peaks centred at $q = 0.68$ Å^{-1} and 1.45 Å^{-1}, while seven crystalline peaks were superimposed onto the two amorphous peaks in the $iPS_{crystalline}$ profile. A volume crystallinity index (χ_v) for the ex-situ iPS samples was determined by separating out the amorphous, crystalline and background contributions to scattering between 0.4 Å^{-1} ≤ q ≤ 4 Å^{-1}, similar to the procedure outlined previously for iPP [39] and using the following equation:

$$\chi_v = \frac{A_{crystalline}}{A_{crystalline} + A_{amorphous}} \quad (1)$$

where $A_{crystalline}$ is the area of the crystalline peaks and $A_{amorphous}$ is the amorphous area. The crystallinity determined by X-ray was χ_v = 23(1)%. The crystallinity determined by DSC was in close agreement $\chi_{v(DSC)}$ = 25(2)%. No crystallinity was observed in $iPS_{amorphous}$ by DSC or X-ray techniques.

3.2. Crystalline morphology

POMs were taken while the iPP was in the molten (200 °C) and crystalline states Fig. 4. During crystallisation the surface of the $iPS_{crystalline}$ particles were covered by a negatively birefringent phase characteristic of β-iPP. Many nucleation points were observed and crystal growth appeared to be columnar. The identification of β-iPP was confirmed by heating the material in-situ. The phase covering the $iPS_{crystalline}$ particle melted at ~155 °C while the surrounding material melted at ~169 °C. Under the same conditions no negatively birefringent phase could be observed in either the iPP($iPS_{amorphous}$) or $iPP_{control}$ samples. The presence of both morphologies of iPS also substantially reduced the α-iPP spherulite size when compared to the $iPP_{control}$.

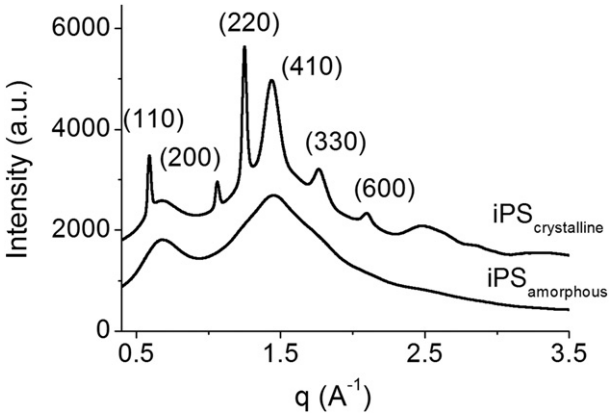

Fig. 3. 1D scattering profiles for ex-situ $iPS_{crystalline}$ and $iPS_{amorphous}$ material.

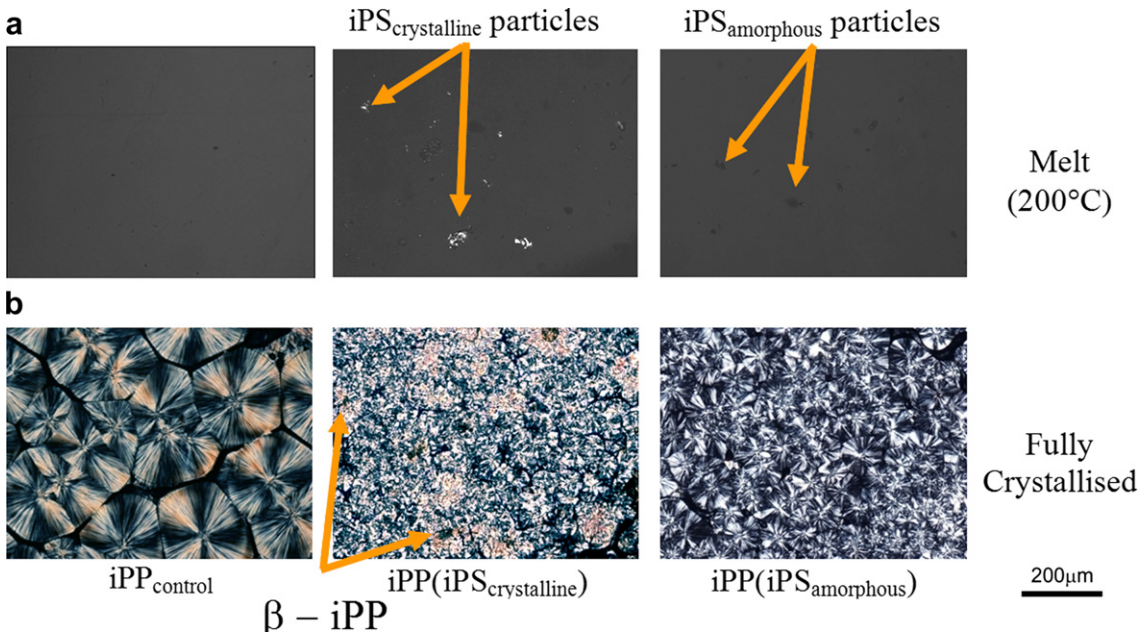

Fig. 4. Polarised optical micrographs taken of (a) the iPP melt and (b) after isothermal crystallisation at 135 °C under quiescent conditions.

1D WAXS profiles after the samples were fully crystallised from the quiescent state and after a moderate step shear are shown in Fig. 5. Automated procedures were employed to deconvolute the scattering profiles using the fityk© software package. Three Gaussian curves centred at $q = 1.0$ Å^{-1}, 1.2 Å^{-1} and 1.45 Å^{-1} were used to account for the amorphous scattering. Seven Gaussian curves were used to account for the major crystalline scattering peaks observed between 0.9 Å$^{-1} \leq q \leq 1.6$ Å^{-1}. The volume crystallinity index was determined using Eq. (1). The relative amount of β phase was determined using the Turner–Jones method [44]:

$$K_\beta = \frac{A_\beta(300)}{A_\beta(300) + A_\alpha(110) + A_\alpha(040) + A_\alpha(130)} \quad (2)$$

where $A_\beta(300)$, $A_\alpha(110)$, $A_\alpha(040)$ and $A_\alpha(130)$ are the areas of the reflections indicated in Fig. 5a. The χ_v and K_β values are presented in Table 1. In the quiescent condition iPP(iPS$_{crystalline}$) contained a mixture of β-iPP ($K_\beta = 0.26$) and α-iPP while both iPP(iPS$_{amorphous}$) and iPP$_{control}$ samples did not show any β-iPP. This supports the POMs shown in Fig. 4. Shearing the melt prior to crystallisation led to all samples having a small amount of β-iPP. The samples containing both morphologies of iPS had essential the same β-iPP contents with $K_\beta \sim 0.08$–0.09, while iPP$_{control}$ had a slightly smaller value $K_\beta = 0.04$.

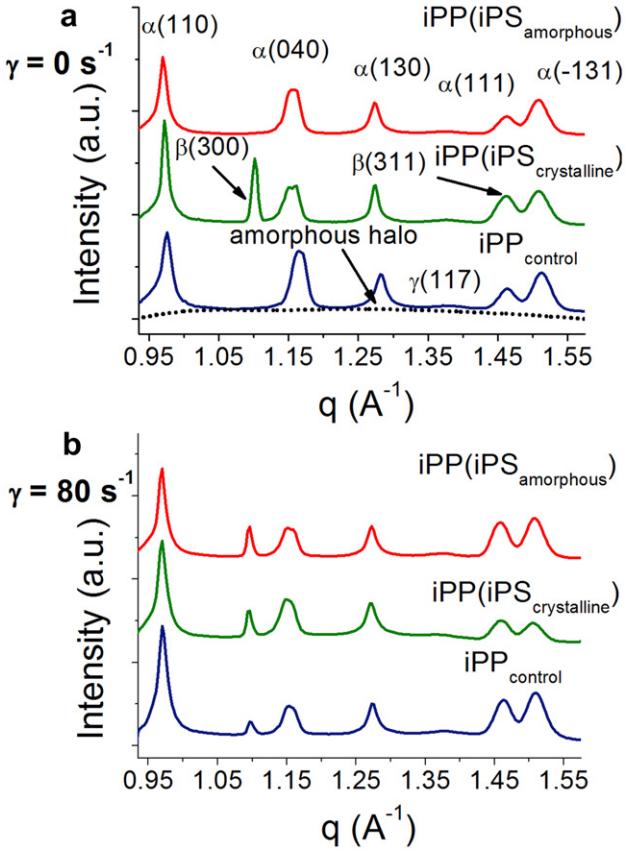

Fig. 5. 1D WAXS profiles of fully crystallised material (a) in the quiescent condition and (b) after a moderate step shear with a shear rate of 80 s^{-1} for 1 s.

2D SAXS patterns after quiescent crystallisation and in the fully crystallised state are presented in Fig. 6a. These patterns show that the lamellar structure produced from quiescent conditions are essentially isotropic. SAXS patterns taken immediately after the application of shear (<5 s) and after crystallisation had come to completion are shown in Fig. 6b and c respectively. For iPP$_{control}$ the step shear resulted in scattering at low angles in the equatorial region immediately after shear. These streaks persisted throughout the crystallisation process and were observed in the final fully

Table 1
Crystallinity index (χ_c), relative amount of beta phase (k_β) crystallisation half time ($t_{0.5}$) and Avrami exponent (n) under quiescent crystallisation conditions and a moderate step shear. Uncertainty in the measurement is recorded as a 95.4% confidence interval.

Material	Condition	χ_c (%)	k_β (%)	$t_{0.5}$ (s)	n
iPP$_{control}$	Quiescent	56(1)	~0	753(8)	3.0(0.2)
iPP(iPS$_{crystalline}$)		63(1)	26(1)	223(3)	2.7(0.1)
iPP(iPS$_{amorphous}$)		53(1)	~0	278(4)	3.1(0.1)
iPP$_{control}$	Sheared	60(1)	4(1)	115(2)	2.4(0.1)
iPP(iPS$_{crystalline}$)		61(1)	8(1)	73(1)	1.9(0.1)
iPP(iPS$_{amorphous}$)		61(1)	9(1)	83(1)	2.0(0.1)

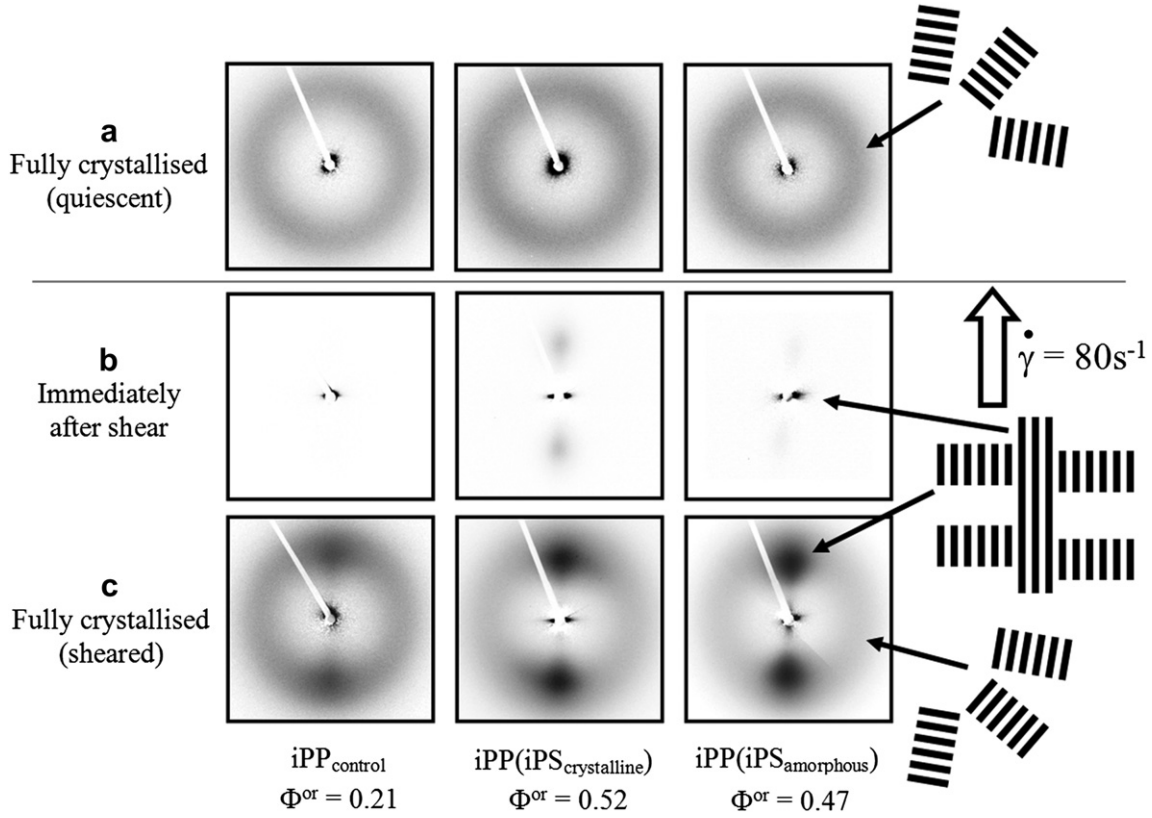

Fig. 6. Two dimensional SAXS images taken (a) in the fully crystallised condition after quiescent crystallisation, (b) immediately after the application of shear, and (c) in the fully crystallised condition after a moderate step shear with a shear rate of 80 s^{-1} for 1 s. Oriented fraction of lamellae (Φ^{or}) is provided for the fully crystallised material after a moderate step shear.

crystallised material. The formation of the streaks was quickly followed by an increase in scattering intensity in the meridional position. This type of scattering is consistent with a shish kebab model [36,37,39], where the equatorial scattering is due to oriented crystal precursors (shish) and the meridional scattering is due to epitaxial nucleated lamellae with their chain axis aligned along the flow direction (kebabs). Isotropic scattering was also observed and is assumed to be due to randomly oriented lamellae. The equatorial scattering formed immediately after shear was much stronger and extended to higher scattering angles for the materials containing both morphologies of iPS. Equally the meridional scattering was more pronounced and there was less isotropic scattering in these samples.

To quantify the amount of oriented lamellae formed, the oriented fraction (Φ^{or}) was determined from the azimuthal integration of background subtracted SAXS data according to the method proposed by Somani et al. [45]:

$$\Phi^{or} = \frac{\text{integrated area due to oriented scattering}}{\text{total integrated area}} \quad (3)$$

where the oriented and un-oriented components of scattering are defined in Fig. 7. It was found that Φ^{or} for the material containing both iPS morphologies was more than twice that of iPP$_{control}$. The material containing iPS$_{crystalline}$ had a slightly higher Φ^{or} than the material containing iPS$_{amorphous}$, although more detailed studies would be needed to test whether this is significant.

3.3. Crystallisation kinetics

The kinetics of crystallisation were probed by plotting the relative crystallinity (χ_{rel}) versus time, Fig. 8. The relative crystallinity was determined by dividing the instantaneous crystallinity (χ_t) by the total crystallinity of the fully crystallised material (χ_∞). Quantitative information about the crystallisation kinetics and growth geometry was obtained by fitting the crystallisation data to the Avrami model.

$$1 - \chi_{rel} = e^{-kt^n} \quad (4)$$

where k is the bulk crystallisation constant and n is the Avrami exponent. The crystallisation half time ($t_{0.5}$) was taken as the time at which the model line intersected $\chi_{rel} = 50\%$. Compared to the iPP$_{control}$, $t_{0.5}$ was dramatically reduced in the presence of both iPS morphologies, with $t_{0.5}$ for iPP(iPS$_{crystalline}$) being slightly less than iPP(iPS$_{amorphous}$), Table 1. The crystallisation kinetics from a sheared melt were significantly faster, up to 6 times for iPP$_{control}$, than for the quiescent condition. The $t_{0.5}$ for both iPS morphologies after the moderate step shear were significantly reduced compared to the iPP$_{control}$. iPP(iPS$_{crystalline}$) had a slightly shorter $t_{0.5}$ than iPP(iPS$_{amorphous}$).

The Avrami exponent was determined in the primary crystallisation region from the gradient of the linear region of a plot of $\ln(\ln(1/1 - \chi_{rel}))$ versus $\ln(t)$. At low conversions there is a significant uncertainty in determining χ_{rel} by the above method. Significant deviation from the model also occurs in the latter stages of crystallisation which has been attributed to the occurrence of secondary crystallisation [46]. Therefore the Avrami exponent was determined by fitting a straight line to the linear region between these two extremes as shown in Fig. 9. In heterogeneous nucleation the Avrami exponent is related to the dimension of crystal growth: with $n = 3$ indicating spherical growth; $n = 2$ indicating disklike growth; and $n = 1$ indicating rodlike growth. Often non-integer values of the Avrami exponent

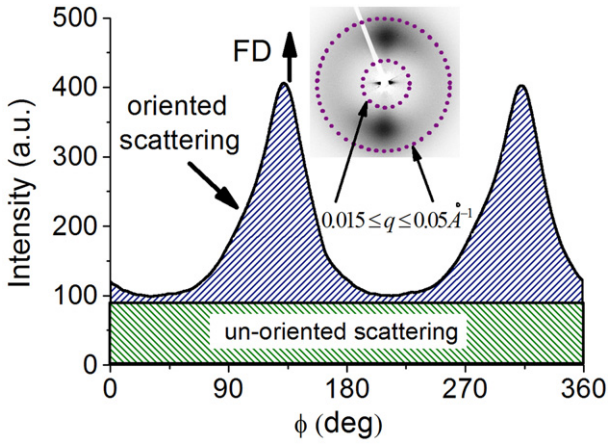

Fig. 7. Plot of background subtracted intensity versus azimuthal angle (ϕ) showing the method used to determine the oriented fraction of lamellae (Φ^{or}) shown in Fig. 6.

are obtained indicating the presence of more the one growth geometry during crystallisation. The Avrami exponents determined by this method are summarised in Table 1. In the quiescent condition both iPP$_{control}$ and iPP(iPS$_{amorphous}$) had Avrami exponents close to 3 which is indicative of the spherulite growth observed in Fig. 4. iPP(iPS$_{crystalline}$) had a slightly smaller exponent ($n \sim 2.7$) which may be due to the observed columnar growth of β-iPP from the surface of the iPS$_{crystalline}$ particles. After the moderate step shear the Avrami exponent of all samples was reduced with iPP$_{control}$ having $n \sim 2.4$ and the iPP containing both morphologies of iPS being close to $n \sim 2$ i.e. disklike growth. This result is consistent with the SAXS results presented in Fig. 6.

3.4. Thermal behaviour

Samples for DSC analysis were sectioned from the fully crystallised disks after the selected thermal–shear profile. The arc was approximately 1 mm along the radius which in the sheared samples corresponded to shear rate range of ~5 s^{-1}. DSC heating scans of the three iPP samples after quiescent crystallisation are shown in Fig. 10a. All samples showed an obvious endothermic peak between 165 °C and 170 °C due to α-iPP. The iPP(iPS$_{crystalline}$) sample showed an additional peak at 156.2 °C which is in the

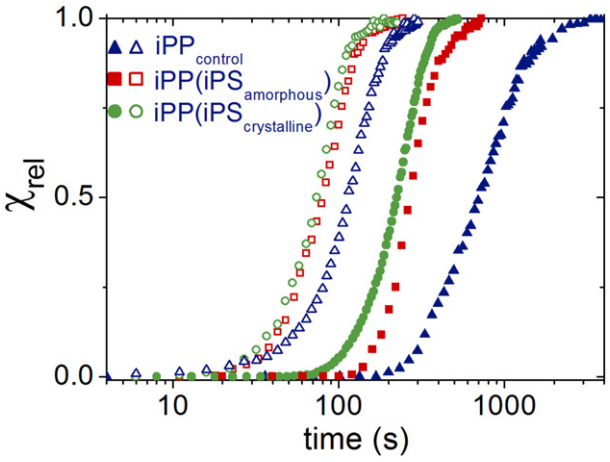

Fig. 8. Relative crystallinity (χ_{rel}) for the three samples during quiescent crystallisation (solid symbols) and after a moderate step shear with a shear rate of 80 s^{-1} for 1 s (open symbols).

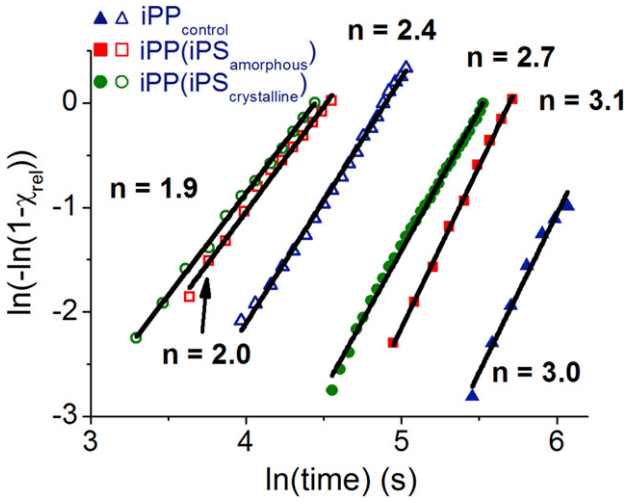

Fig. 9. Avrami plots of the crystallisation data for the three samples during quiescent crystallisation (solid symbols) and after a moderate step shear with a shear rate of 80 s^{-1} for 1 s (open symbols).

temperature range for β-iPP. The application of a moderate step shear complicated the heating scans further, Fig. 10b. All samples showed a similar sized shallow peak in the β-iPP temperature range at ~155 °C. The α-iPP peaks of iPP(iPS$_{crystalline}$) and iPP(iPS$_{amorphous}$) samples split into at least two separate endothermic peaks. It is suggested that the different lamellar components arising from oriented and un-oriented α-iPP crystals are responsible for the two peaks. However, multiple melting peaks are not uncommon in α-iPP and their designation remains to be confirmed. A small peak in the melting profiles at higher temperatures (~225 °C) due to the 2 wt% crystalline iPS was observed in both the sheared and un-sheared iPP(iPS$_{crystalline}$) samples. The position and area of these peaks were consistent with the presence of 2 wt% iPS$_{crystalline}$.

4. Discussion

4.1. Morphology of iPS

Like most polymer pairs, on blending, polypropylene and polystyrene are essentially immiscible. This results in the iPS remaining as discrete particles at the end of both heat treatments. Ex-situ X-ray analysis of material which had been given essentially the same thermal profile as experienced in the shear cell shows that the crystallinity of the iPS$_{crystalline}$ particles was reasonably high at (χ_v = 23(1)%) while iPS$_{amorphous}$ particles showed no discernable crystallinity. The particle morphology of the originally crystalline iPS particles was irregular. Their morphology is however only slightly altered by heating them above their melting point where they tend to become more spherical. The crystalline order observed at the lower temperature is destroyed, and due to the sluggish crystallisation kinetics of iPS, they remain essentially amorphous during the subsequent isothermal crystallisation of iPP. This was confirmed by the DSC measurements presented in Fig. 10.

The non-polar methyl groups on iPP molecules would interact with iPS through their phenyl groups [26]. Therefore, the arrangement of phenyl groups in the crystal and amorphous state is important in understanding how the morphology of iPS would influence the crystallisation of iPP. Crystalline iPS has been shown to form a 3_1 helix with a rhombohedral unit cell (on hexagonal parameters $a = b = 21.90$ Å and $c = 6.65$ Å) [35]. The phenyl groups within this crystal structure form into parallel stacks with the

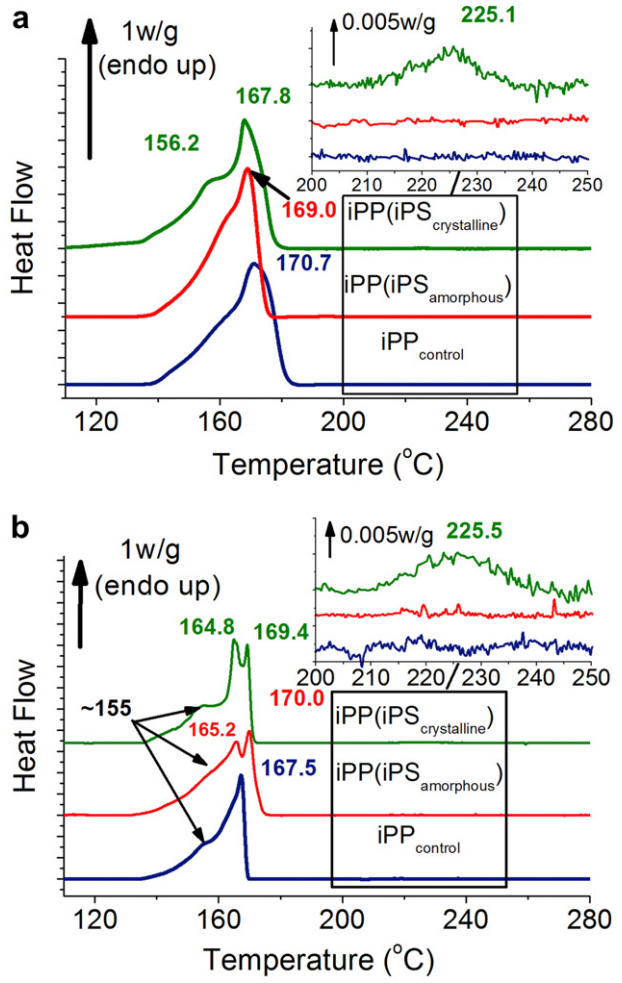

Fig. 10. Ex-situ DSC heating scans after (a) quiescent crystallisation and (b) after a moderate step shear with a shear rate of 80 s^{-1} for 1 s. The insert is a magnification of the high temperature region from 200 °C to 250 °C.

repeat distance between adjacent phenyl groups within the same stack being 6.65 Å apart.

Amorphous iPS also shows considerable short range order due to the steric interactions of the bulky phenyl groups dominating chain conformation and packing. This ordering is evident by the two broad peaks centred at $q = 0.68$ $Å^{-1}$ (polymerisation peak) and 1.45 $Å^{-1}$ (amorphous halo) in the WAXS profiles shown in Fig. 3. The conformation of the polystyrene chains in the amorphous state has been extensively studied, primarily by diffraction techniques [28–32]. By comparing experimentally derived radial distribution function (RDF) with those calculated from structural models, early studies, such as those by Katada [28], Yeh [29], Wecker et al. [30] and Schubach et al. [31] suggested the PS chains undergo orderly packing with neighbouring chains being roughly parallel to one another. The distance between adjacent chains was thought to be about 9–10 Å, while the distance between adjacent phenyl groups on the same chain, as well as between neighbouring chains was ~5 Å. Adams el al. performed a detailed conformational study of amorphous PS and indicated that this type of packing could be achieved if the chain adopted a disordered helical arrangement [32], although, the conformational parameters presented were in contradiction to those indicated by conformational energy calculations [33]. Even though these models could explain broadly the features of the scattering profile of amorphous PS, they could not account for the unusual position and temperature dependence of the polymerisation peak which increases in intensity with increasing temperature. This issue was overcome by the super chain model proposed by Mitchel and Windle [34]. In their model, micro-segregation of the phenyl groups occurs whereby the phenyls form into stacks as if they were flexible super chains. The stacks are similar to that found in crystalline iPS, being locally parallel to one another but are more highly disordered. The backbone does not form a helix but rather adopts a random configuration with as many as 6 chain segments being able to contribute to the same region of the stack. The distance between adjacent phenyls in the stacks is ~5 Å, and the distance between adjacent super chains is ~9 Å. Transmission electron microscopy suggests that the ordered regions range in size from 15 to 45 Å [29]. It should be emphasised here that the order found in amorphous iPS is not long range in the accepted meaning of the term.

4.2. Crystallisation from a quiescent melt

The experimental results show that the presence of both morphologies of iPS substantially influenced the quiescent crystallisation of iPP. $iPS_{crystalline}$ particles were covered by β-iPP but their presence also increased the overall crystallisation kinetics and resulted in a substantial decrease in the spherulite size of α-iPP spherulites further away from the particles. $iPS_{amorphous}$ particles did not induce β-iPP. However, like $iPS_{crystalline}$ their presence also resulted in increased crystallisation kinetics and smaller α-iPP spherulite size. Therefore it can be concluded that morphologically, $iPS_{crystalline}$ selectively nucleates β-iPP and $iPS_{amorphous}$ nucleates α-iPP. While kinetically, both $iPS_{crystalline}$ and $iPS_{amorphous}$ increase the crystallisation rate of iPP with the influence of $iPS_{crystalline}$ on crystallisation kinetics of iPP being more significant.

One possible explanation for these results is as follows: the conformational changes that occur to the iPS molecule during crystallisation result in a change in the epitaxial relationship between iPS and iPP. In helical polymers such as iPP it is considered that there are two possible ways a substrate can interact with the helix: a) via the interstrand distance as found in α-iPP & γ-iPP or b) by the repeat distance between adjacent chains as found in β-iPP [24]. The contact plane of α-iPP (010) consists of a lozenge shaped array of methyl groups [25]. Compounds with substantially different repeat distances have been found to interact with this array and act as effective α-iPP nucleants (4.2 Å, 5.0 Å, and 6.6 Å) [25]. β-iPP on the other hand has been found to interact with only one repeat distance (~6.5 Å) but it also requires an orthogonal cell geometry [24,27]. In this case it is though that the ~5.0 Å repeat distance between adjacent phenyls in $iPS_{amorphous}$ would lead to nucleation of α-iPP while the 6.65 Å repeat distance between adjacent phenyls in $iPS_{crystalline}$ would lead to nucleation of β-iPP.

4.3. Crystallisation from a sheared melt

Over the last few years considerable effort has been focused on understanding the formation of oriented crystal precursors in sheared polymer melts. The addition of nucleating agents further complicates the process. However, a detailed explanation for the influence of nucleating agents on the formation of oriented crystal precursors is yet to be determined. In this experiment, a considerably greater intensity and an extension to high scattering angles values of the sharp equatorial streak was observed immediately after the application of shear in the presence of both iPS morphologies. This can be interpreted by an increase in the density of oriented crystal precursors. It is believed that both morphologies of the iPS particle could lead to this increased number of oriented crystal precursors in at least three ways: 1) it could increase the local strain rate in the area adjacent to the nucleating particle similar to the way

a log increases the local flow rate in a fast running stream; 2) one end of the iPP molecule could get adsorbed onto the surface of the iPS particle, while the free end gets stretched by the flow; and 3) the surface of the iPS particles could stabilise oriented molecules in the melt preventing them from relaxing back to their coiled state. The aligned segments could then drift together as suggested by Dukovski and Muthukumer [47] to form an overlap region in the flow field which could then spread over the entire chain.

The application of shear led to a similar β phase content for all three samples. Sheared melts are widely known to encourage the formation of β-iPP. It has been shown that an α to β growth transition or α β bifurcation occurs on the surface of α-iPP row nuclei [13]. Nevertheless, the nature of the nucleation sites responsible for β-iPP nucleation is still under debate. Sun et al. suggested that an orientation window exists for the iPP molecule in the molten state which enables the nucleation of β-iPP [12]; while Li et el. argued that shear can induce the formation smectic ordered domains, and that growth of β-iPP should be easier than α-iPP from these shear-induced smectic bundles [48]. Although the application of the step shear resulted in the formation of β-iPP for $iPP_{control}$ and iPP($iPS_{amorphous}$) samples, the step shear decreased the β phase content for iPP($iPS_{crystalline}$) material, Fig. 5. The selective nucleation of β-iPP from $iPS_{crystalline}$ particles observed during quiescent crystallisation is therefore seemingly suppressed by the step shear. Similar behaviour has been observed by Huo et al. [18] who used WAXS and POM to investigate the influence of shear rate on the β content of an iPP nucleated by selective β nucleating agent (LaC + $CaCO_3$). Hou argued that shear increases the number of α crystal precursors which selectively nucleate α phase. This seemed to be at odds with the well known increase in β phase content during shear-induced crystallisation of iPP that occurs through α β bifurcation [11–13]. Therefore it was unclear whether shear, in the presence of a selective β-iPP nucleating agent, suppressed the formation of oriented α crystals or instead promoted them to the extent that that β phase growth from α β bifurcation would be unfavourable.

The results presented here show that the addition of both morphologies of iPS considerably increased the number of oriented crystal precursors that form immediately after the application of shear. As shown by the increase in crystallisation kinetics, which are significantly faster than found in the quiescent condition, these oriented crystal precursors are very effective at nucleating α-iPP. Therefore their presence completely overwhelms the crystallisation process, resulting in high proportions of oriented α form crystals. These results therefore have important implication for the processing of iPP containing intentional β-iPP nucleants, the addition of which can influence both the level of orientation achieved as well as the β phase content.

5. Conclusion

The morphology of isotactic polystyrene (iPS) particles which had been added to a matrix of isotactic polypropylene (iPP) were successfully varied by heat treatment to be either semicrystalline ($iPS_{crystalline}$) or amorphous ($iPS_{amorphous}$). Isothermal crystallisation of iPP in the presence of iPS particles of both morphologies, (iPP($iPS_{crystalline}$) and iPP($iPS_{amorphous}$)), and a control ($iPP_{control}$) were then studied under quiescent conditions as well as after a moderate step shear. Under quiescent conditions $iPS_{crystalline}$ was found to selectively nucleate the β-iPP while $iPS_{amorphous}$ was found to nucleate α-iPP. During crystallisation from a moderate step shear, both morphologies of iPS resulted in similar amounts of β-iPP and in increased crystallisation kinetics in comparison to $iPP_{control}$. Furthermore, both iPS morphologies were found to substantially increase the number of oriented crystal precursors, compared to $iPP_{control}$ which were formed as a result of the shear. These oriented precursors ultimately swamp the effect of any nucleating agent present and promote the formation of oriented α form lamellae.

Acknowledgements

This work was performed at the SAXS/WAXS beamline at the Australian Synchrotron, Victoria, Australia and the Australian National Beamline Facility (ANBF) with support from the Australian Synchrotron Research Program, which is funded by the Commonwealth of Australia under the Major National Research Facility Program. The Authors would like thank Dr Stephen Mudie, Dr Nigel Kirby and Dr Adrian Hawley for their assistance with the synchrotron experiments and modification of the SAXS15id software.

References

[1] Natta G, Corradini P. Il Nuovo Cimento 1960;15(1):40–51.
[2] Meille SV, Ferro DR, Brueckner S, Lovinger AJ, Padden FJ. Macromolecules 1994;27(9):2615–22.
[3] Dorset DL, McCourt MP, Kopp S, Schumacher M, Okihara T, Lotz B. Polymer 1998;39(25):6331–7.
[4] Padden FJ, Keith HD. Journal of Applied Physics 1959;30:1479–84.
[5] Addink EJ, Beintema J. Polymer 1961;2:185–93.
[6] Kortek J, Raab M, Baldrian J, Grellmann W. Journal of Applied Polymer Science 2002;85(6):1174–84.
[7] Varga J. Journal of Macromolecular Science Part B Physics 2002;41(4):1121–71.
[8] Karger-Kocsis J. Polypropylene. An A–Z reference. Great Britain: Kluwer Academic Press; 1999. p. 58.
[9] Lovinger AJ, Chua JO, Gryte CC. Journal of Polymer Science Polymer Physics Edition 1977;15(4):641–56.
[10] Thomason JL, Van Rooyen AA. Journal of Materials Science 1992;27(4):897–907.
[11] Somani RH, Hsiao BS, Nogales A, Fruitwala H, Srinivas S, Tsou AH. Macromolecules 2001;34(17):5902–9.
[12] Sun X, Li H, Wang J, Yan S. Macromolecules 2006;39(25):8720–6.
[13] Varga J, Karger-Kocsis J. Journal of Polymer Science, Part B: Polymer Physics 1996;34(4):657–70.
[14] Liu G, Zhu PW, Edward G. Macromolecular Symposia 2002;185:327–40.
[15] Huo H, Jiang S, An L. Polymer 2005;46(24):11112–6.
[16] Chen YH, Zhong G-J, Wang Y, Li Z-M, Li L. Macromolecules 2009;42(12):4343–8.
[17] Ma CG, Chen L, Xiong XM, Zhang JX, Rong MZ, Zhang MQ. Macromolecules 2004;37(24):8829–31.
[18] Huo H, Jiang S, An L. Macromolecules 2004;37:2478–83.
[19] Varga J, Mudra I, Ehrenstein GW. Journal of Applied Polymer Science 1999;74(10):2357–68.
[20] Varga J. Journal of Thermal Analysis 1989;35:1891–912.
[21] Dong M, Guo Z, Su Z, Yu J. Journal of Polymer Science, Part B: Polymer Physics 2008;46(12):1183–92.
[22] Su ZQ, Chen XN, Yu ZZ, Zhang L. Journal of Applied Polymer Science 2009;111(2):786–93.
[23] Su ZQ, Dong M, Guo Z, Yu J. Macromolecules 2007;40(12):4217–24.
[24] Stocker W, Schumacher M, Graff S, Thierry A, Wittmann JC, Lotz B. Macromolecules 1998;31(3):807–14.
[25] Mathieu C, Thierry A, Wittmann JC, Lotz B. Polymer 2000;41(19):7241–53.
[26] Khanna YP. Macromolecules 1993;26(14):3639–43.
[27] Mathieu C, Thierry A, Wittmann JC, Lotz B. Journal of Polymer Science, Part B: Polymer Physics 2002;40(22):2504–15.
[28] Katada K. Acta Crystallographica 1963;16(4):290–301.
[29] Yeh GSY. Journal of Macromolecular Science Part B Physics 1972;6(3):451–63.
[30] Wecker SM, Davidson T, Cohen JB. Journal of Materials Science 1972;7(11):1249–59.
[31] Schubach HR, Nagy E, Heise B. Colloid and Polymer Science 1981;259(8):789–96.
[32] Adams R, Balyuzi HHM, Burge RE. Journal of Materials Science 1978;13(2):391–401.
[33] Yoon DY, Sundararajan PR, Flory PJ. Macromolecules 1975;8(6):776–83.
[34] Mitchell GR, Windle AH. Polymer 1984;25(7):906–20.
[35] Natta G, Corradini P, Bassi I. Il Nuovo Cimento 1960;15(1):68–82.
[36] Kimata S, Sakurai T, Nozue Y, Kasahara T, Yamaguchi N, Karino T, et al. Science 2007;316(5827):1014–7.
[37] Somani RH, Yang L, Zhu L, Hsiao BS. Polymer 2005;46(20):8587–623.
[38] Kumaraswamy G. Journal of Macromolecular Science, Part C: Polymer Reviews 2005;45(4):375–97.
[39] Zhu PW, Tung J, Phillips A, Edward G. Macromolecules 2006;39(5):1821–31.
[40] Zhu PW, Phillips A, Tung J, Edward G. Journal of Applied Physics 2005;97(10):104908.
[41] Zhu PW, Edward G. Macromolecules 2004;37(7):2658–60.
[42] Liu T, Petermann J. Polymer 2001;42(15):6453–61.

[43] Hui Xu B, Ince S, Cebe P. Journal of Polymer Science, Part B: Polymer Physics 2003;41(23):3026–36.
[44] Turner-Jones A, Cobbold AJ. Journal of Polymer Science 1968;6(8):539–46.
[45] Somani RH, Hsiao BS, Nogales A, Srinivas S, Tsou AH, Sics I, et al. Macromolecules 2000;33:9385–94.
[46] Mubarak Y, Harkin-Jones EMA, Martin PJ, Ahmad M. Polymer 2001;42(7):3171–82.
[47] Dukovski I, Muthukumar M. The Journal of Chemical Physics 2003;118(14):6648–55.
[48] Li L, de Jeu WH. Faraday Discussions 2005;128:299–319.